Research Article

Open Access

Andrzej Pytlik*, Witold Frąc

Safety of Steel Arch Support Operation During Rock Bursts Under Explosive Atmosphere Conditions

https://doi.org/10.2478/sgem-2023-0004
received September 24, 2021; accepted January 5, 2023.

Abstract: Methane and coal dust explosions are among the most common causes of disasters in hard coal mining. Therefore, it is important for occupational safety in hard coal mines operating under methane and coal dust explosion hazards to identify possible ignition sources, whether due to natural or technical factors. One technical source of ignition can be mechanical sparks generated during operation of mechanical equipment and high surface temperatures of equipment components during operation. This paper presents the methodology and results of thermal imaging and strength testing of roadway support elements under dynamic loading. The goal of the tests was to identify the potential explosive atmosphere ignition sources during the operation of the support under the conditions of rock bursts. The scope of testing encompassed the temperature measurements by means of thermal camera of friction prop and yielding support frame sliding joint elements at yield under dynamic impact loading (simulating a burst). Significant joint element heating and mechanical sparking was observed during the testing of arching yielding support frame sliding joints and straight friction prop joints as a result of friction at yield. Some of the aspects defined in standard PN-EN ISO80079-36:2016 include the maximum temperature T max =150°C for a surface that can accumulate a layer of coal dust. Tests of the friction joints have shown that during impact loading, numerous mechanical sparks are produced at the friction joints of sections of the steel prop, with the surface temperature of the sections starting from 169.6°C and reaching up to 234.1°C. During tests it was also to determined emissivites of the tested sliding joints constructed from V29-V32 secrions depending on corrosion products which consist in range 0.842-0.873. Such a high temperature can initiate an explosive mixture consisting of methane, air and coal dust.

***Corresponding author: Andrzej Pytlik,** Główny Instytut Górnictwa: Glowny Instytut Gornictwa, Katowice, Poland, E-mail: apytlik@gig.eu; ja.pytlik@gmail.com
Witold Frąc, Główny Instytut Górnictwa: Glowny Instytut Gornictwa, Katowice, Poland

Keywords: arching support sliding joints; straight prop sliding joints; dynamic load capacity; kinetic coefficient of friction; thermal imaging.

1 Introduction

The constant increase in the extraction depth and concentration of output in hard coal deposits is one of the primary reasons for the rising absolute methane emission rates and coal seam methane pressure in mining plants (Cybulski et al., 2018). It has a direct influence on the increase in methane explosion hazards present in deep mines. Coal dust and methane explosions are some of the most common causes of mining disasters in hard coal mines all over the world, and research continues to be conducted with the purpose of understanding the mechanisms of explosion as well as improving explosion prevention, monitoring and risk reduction (Shepherd et al., 1981; Takla & Vavrusak, 1999; Cioca & Moraru, 2012; Hudeček et al., 2012; Shao & Ma, 2012; Brune, 2013; Krause & Smoliński, 2013; Li et al., 2013; Hao et al., 2014; Krause & Skiba, 2014; Yuan, 2016; Trenczek, 2015; Burtan et al., 2017; Song et al., 2021). Broad-scale research has been conducted in Poland and worldwide for many years to reduce the risk of methane and coal dust explosion, with the intent of drafting protection standards and developing methods for explosion mechanism identification and prevention and ignition source detection (Pytlik et al., 2021). The introduction of electrical equipment into mining plants in 1870 necessitated the commencement of research on explosion hazards (Górny, 2013). It should be noted that the first studies on the parameters that determine methane ignition were conducted in Germany as early as 1884–1885, whereas the first fireproof shield tests were carried out at the University of Sheffield. This work resulted in regulations and standards being issued in countries such as Germany and the UK. The first standard organisation with an international reach was the International Electrotechnical Commission (IEC), established in 1906. In Poland, the first standard

concerning explosion-proof equipment was issued in 1929 by the Association of Polish Electrical Engineers (Stowarzyszenie Elektryków Polskich [SEP]), in cooperation with the Czechoslovakian Electrotechnical Association (Elektrotechnický Svaz Československý [ESČ]). The research institution named the Experimental Mine 'Barbara', the Central Office of Mining Rescue and the Magnetic Observatory in Mikołów was established nearly 100 years ago (in 1925), and some of its activities included the testing of devices, equipment and materials used in mines, as well as research on gas and coal dust explosion phenomena. Currently, the Experimental Mine 'Barbara' is a part of the Central Mining Institute in Poland. The testing grounds of the Experimental Mine 'Barbara' constitute the only site in Europe that is capable of accommodating full-scale gas and dust explosion tests.

In order to standardise the regulations concerning basic requirements for equipment intended for use in explosive atmospheres, the European Union member states adopted the ATEX Directive 2014/34/EU (Eckhoff, 2006; Petitfrere & Proust, 2006; Jespen, 2016). Before a device is permitted for use in the field, it is important to carry out its conformity assessment process, part of which involves tests for conformity with standards harmonised with the ATEX directive. Should no harmonised standards exist, the required tests and extent of testing are determined by a body notified within the scope of the directive, and some of the basic certification tests include maximum temperature determination and potential methane and coal dust ignition source identification (Kałuża, 2017; Jurca et al., 2020). The ATEX directive encompasses requirements for both electrical and non-electrical (Rogers, 2003; Gakhar et al., 2006; Thurnherr et al., 2007; Ghicioi et al., 2010a and 2010b; Jurca et al., 2020) devices. Unlike electrical device standardisation, the standardisation of non-electrical devices is a relatively recent endeavour, and its greatest development began with the adoption of the ATEX directive in 1994 (Górny, 2017).

One technical source of ignition of methane can be mechanical sparks, resulting from friction of rocks between each other as well as during operation of mechanical equipment, and the high surface temperature of equipment components during their operation in an explosive atmosphere. (Cioca & Moraru, 2012; Trenczek, 2015; Prostański, 2018; Pytlik et al., 2021; Song et al., 2021; Zhang et al., 2021). The issue of where the mechanical sparks are formed on the steel support and the formation of high-temperature areas, which can pose a risk of ignition of an explosive gas mixture, is poorly recognised, as is also indicated by the small literature in this area.

Initial tests of straight sliding joints constructed from V29 sections under static and dynamic loading were presented in a publication concerning loads exerted on the support by a suspended monorail system (Pytlik, 2019a). The mechanical sparking phenomenon observed during the tests motivated the author to continue the research on full-scale support frames (Pytlik, 2019b; Pytlik, 2020) to better understand the surface temperature generated as a result of arching sliding joint yield and to determine the locations of sparking.

This paper presents the methodology and results of thermal imaging and strength testing of straight and arching roadway support sliding joints constructed from V32 sections under dynamic loading. Tests of friction joints were carried out in 2020 and are a continuation of the tests that were the subject of Pytlik's (2020) article, which consists of the load capacity of steel arch support under static loading and friction straight joints under dynamic loading with a maximum impact energy of 28 kJ (according to PN-G-15533:1997) including thermal imaging tests. In this article, the testing of friction joints has been extended, compared to the requirements of the Polish standard (PN-G-15533:1997), to include dynamic testing on curved elements, and the maximum impact energy of the drop mass during testing of friction prop has been increased to approx. 50 kJ at an impact velocity of approx. 2.8 m/s. The research was carried out to identify areas of mechanical spark formation (using a thermal imaging camera) and to determine at what energy and impact velocity the permissible temperature of 150ºC of the section surface is exceeded during sliding under conditions simulating rock burst. The main objective of the study of friction joints under dynamic (impact) loading simulating rock burst, presented in this article, is to identify possible sources of ignition of explosive atmospheres during impulsive loading of a yielding steel arch support under rock burst conditions. This research is new to the extensive studies of friction joints presented by Brodny (2012a and 2012b) and other researchers (Ciałkowski, 1996; Pacześniowski and Pytlik, 2008; Horyl et al., 2014, 2017 and 2019), which were mainly focused on determining the resistance of friction joints under static and dynamic loading.

Compared to the previous dynamic sliding joint testing, the presented work was expanded with arching element tests to better understand the phenomena that occur during yielding. The primary purpose of the tests under dynamic loading was to identify the potential explosive atmosphere ignition sources during the impact loading of the yielding steel arch support under the conditions of rock bursts. The scope of testing encompassed temperature measurements of support sliding joint elements at yield.

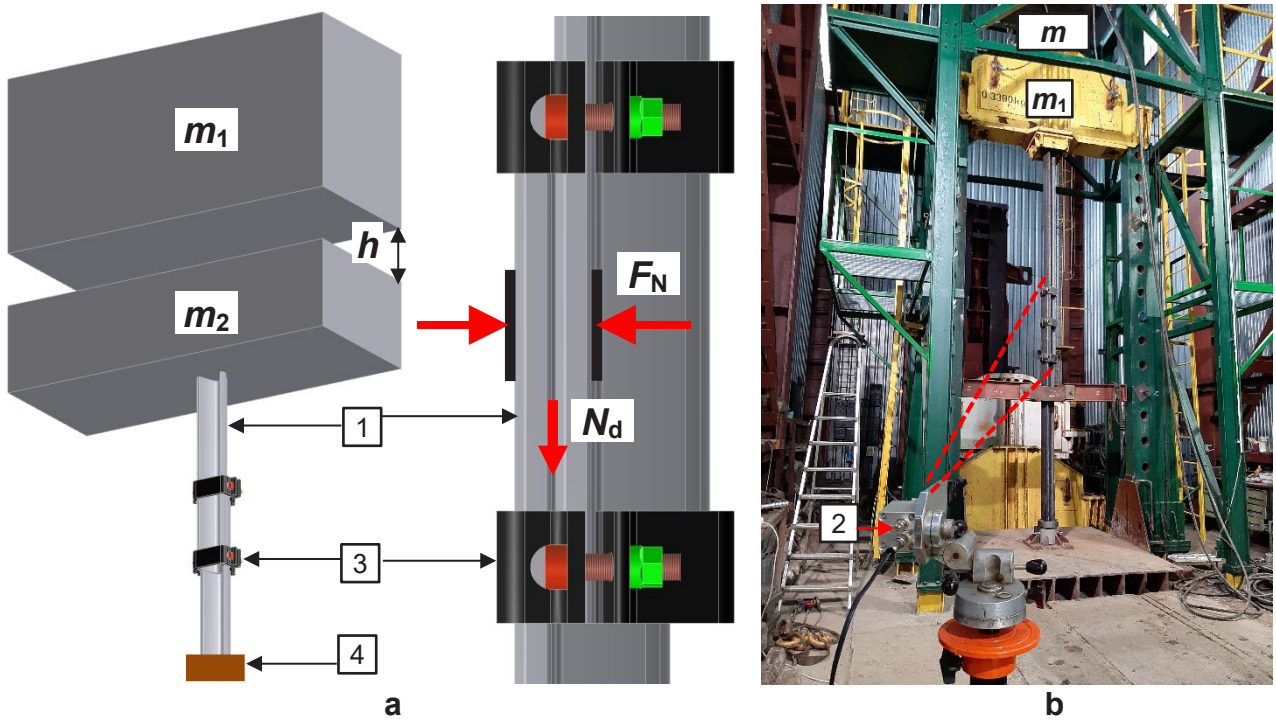

1 – sliding joint; 2 – thermal camera; 3 – shackle for coupling V sections; 4 – force sensor

Figure 1: Setup for testing straight and arching sliding joints (a) and picture of the test facility with an SV prop constructed from V32 sections (b).

Thermal imaging measurements were carried out by means of a high-speed camera with a refresh rate of 128 Hz. The obtained information regarding the temperature distribution in the joint at yield is necessary to identify the locations that influence the increase in frictional resistance or indicate the risk of support element failure. Determining the maximum surface temperature generated as a result of the sliding joint yield makes it possible to inspect whether the maximum temperature defined in standard PN-EN ISO 80079-36:2016 has not been exceeded. The standard in question is harmonised with the ATEX directive concerning group I non-electrical equipment used in explosive atmospheres. Some of the aspects defined in the standard include the maximum temperature T_{max} = 150°C for a surface that can accumulate a layer of coal dust.

2 Materials and Methods

Yielding support frames and friction props are assembled using elements constructed from open V32 sections (or other sections, e.g. with V, TH or U profiles) coupled via overlaps by means of screw pin shackles. Yielding frames and props are commonly utilised at great mining depths under difficult geological and mining conditions resulting from increased rock mass stress and dynamic phenomena in the form of rock mass tremors and rock bursts. Straight and arching sliding joints constructed from V32 sections (PN-H-93441-3:2004) with increased mechanical properties of steel (R_e ³ 550 MPa, R_m ³ 730 MPa) were selected for the tests. Fig. 1 presents a diagram and a picture of the GIG drop hammer testing facility intended for the tests of various types of mine support system elements, that is, roadway support friction props, powered support hydraulic props, ropes, rock bolts and chains, as well as geoengineering elements, that is, micropiles, soil nails and rock anchors.

The methodology for testing ŁP frame and SV friction prop sliding joints under dynamic impact loading was developed based on the following assumptions:

- The dynamic loading of the support frame and friction prop joints is exerted by the impact of masses of rock, resulting from a rock burst (Dubiński & Konopko, 2000).
- The collision of the ram against the crosshead with a velocity v_0 is fully inelastic – after the collision, the ram of a mass m_1 comes into contact with the crosshead of a mass m_2 (exerting static loading on the joint), which remains in permanent contact with the tested sliding joint. Following the collision, the combined masses move jointly with a velocity v_p adopted as the velocity of the impact against the joint.

The impact velocity v_0 of the ram against the crosshead, which exerts static loading on the joint before the impact, is calculated using the following equation:

$$v_0 = \sqrt{2gh}, \tag{1}$$

where: g is the gravitational acceleration and h is the ram height of fall in metres.

Following the collision, the combined masses move jointly with a velocity v_p calculated using the following equation:

$$v_p = v_0 \frac{m_1}{m_1+m_2}. \tag{2}$$

The kinetic energy of the combined masses m_1 and m_2 is

$$E_k = \frac{1}{2}(m_1 + m_2)v_p^2. \tag{3}$$

Applying Equations (1) and (2) to Equation (3) yields the following equation:

$$E_k = h\frac{m_1^2}{m_1+m_2}\mathrm{g}. \tag{4}$$

After the collision, the joint undergoes a yield of z, which results in a change to the combined mass potential energy, calculated from the following equation:

$$E_p = (m_1 + m_2)gz, \tag{5}$$

where z is the joint yield length in metres.

The total mechanical energy E_c of the combined masses participating in the collision, corresponding to the joint dynamic strength, is calculated using the following equation:

$$E_c = E_k + E_p. \tag{6}$$

The joint dynamic load capacity is calculated using the following equations:

$$N_d = \frac{E_c}{z} \tag{7}$$

$$N_d = \frac{m_1^2}{m_1+m_2}\mathrm{g}\frac{h}{z} + (m_1 + m_2)\mathrm{g}. \tag{8}$$

The kinetic coefficient of friction m_d at joint yield under dynamic loading is calculated using the following equation:

$$\mu_d = \frac{N_d}{F_c} \tag{9}$$

where F_c is the total pressure force on the sections in the joint, calculated as the sum of the tension F_N of all the screw pins in the joint, determined using the following equation:

$$F_c = \sum F_N. \tag{10}$$

For example: for three shackles in the joint, the number of pins is six, whereas for four shackles, it is eight pins. The screw pin tension force generated by a torque applied by means of a GEDORE torque wrench is determined using the calculation tables provided by the wrench manufacturer, based on the DIN 13 standard, assuming a coefficient of friction of 0.14 for a new screw thread with no lubrication. The dynamic tests utilised a ram with a mass m_1 = 4070 kg and a crosshead with a mass m_2 = 3300 kg, exerting static loading on the joint before the impact. Given that the maximum surface temperature of the elements must be determined as per standard PN-EN ISO 80079-36:2016, the sliding joint tests employed a thermal camera type PI 230 from OPTRIS with a detector resolution of 160 × 120 pixels, which recorded the courses of the tests with a refresh rate of 128 Hz, thermal sensitivity of 0.3 K and accuracy of ±2°C. The emissivity e of the steel used to construct the V32 sections, exhibiting various states of corrosion (Horst et al., 2018), was determined by comparing their known temperature to the thermal camera readings. For this purpose, short V32 section fragments were heated in a dryer to a known temperature of 100°C, 150°C and 200°C, and afterwards, the emissivity e in the camera was selected in such a way so as to match it with the temperature readings in the dryer. An example picture of V29 and V32 sections (in various states of corrosion) and a thermal image during the inspection of a temperature of 150.2°C set in the dryer are presented in Fig. 2.

The determined emissivities were as follows:
ε = 0.842 – for a slightly corroded V29 section,
ε = 0.863 – for a slightly corroded V32 section,
ε = 0.873 – for a strongly corroded V32 section (arching element) with visible tarnish and flaking corrosion products.

The axial force exerted on the joint during the free fall of the ram was measured during the tests by means of a C6A strain gauge force sensor (class 0.5) connected to a measuring amplifier of the MGCplus type from Hottinger Brüel & Kjær The joint yield z was measured before and after testing using a tape measure. The shackle screw nuts were tightened using a GEDORE torque wrench with a measurement accuracy of ±3%.

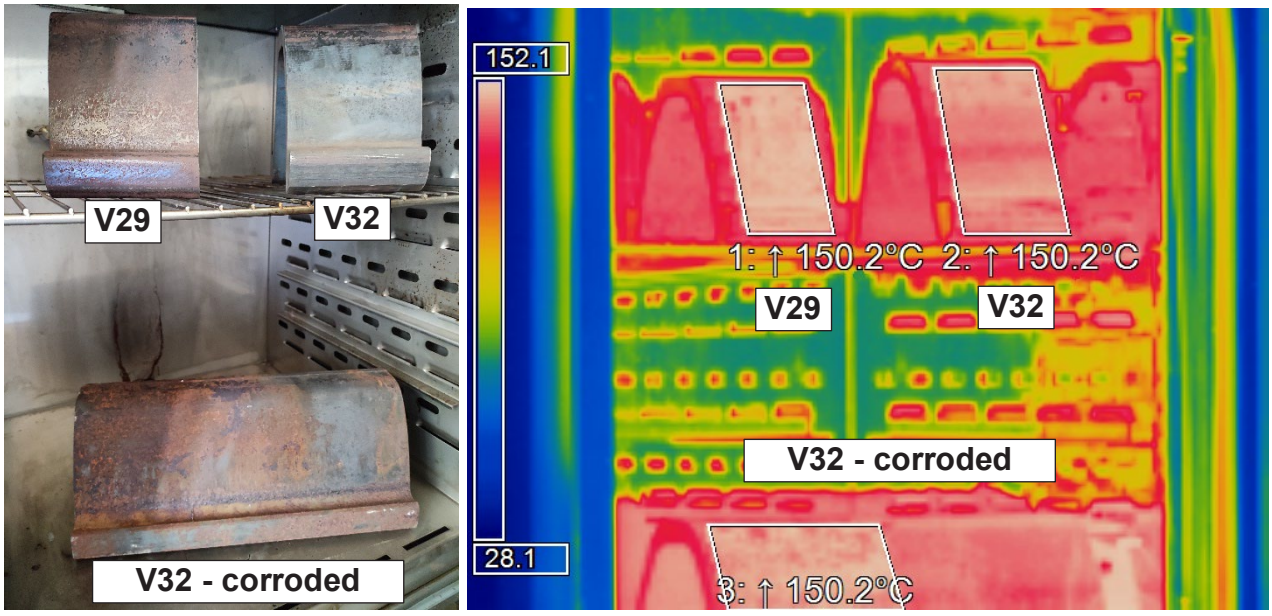

1 – slightly corroded V29 section; 2 – slightly corroded V32 section; 3 – strongly corroded V32 section: tarnish and flaking corrosion products

Figure 2: Inspecting the emissivity e of the steel used to construct the V32 sections: (a) picture of the dryer with the sections; (b) thermal image.

3 Results and Discussion

The dynamic sliding joint load capacity tests were performed based on a methodology for dynamic sliding joint strength testing (PN-G-15533:1997; Pacześniowski & Pytlik, 2008). The straight and arching sliding joints were constructed from V32 sections with enhanced mechanical properties. The test methodology was based on the free fall of a drop mass (ram) m_1 = 4070 kg from a height h onto a crosshead with a mass m_2 = 3300 kg, which exerted static loading on the (straight or arching) joint mounted in the test facility. The height h was gradually increased over a range of h = 0.05-1.3 m, which corresponded to the range of the impact velocity v_p = 0.55-2.75 m/s against the joint. Before testing, the SDO36W shackle screw nuts were tightened with a torque M_d = 450-500 N m, which corresponded to the tension force of a single screw pin, with a value of 102 kN (M_d = 450 N m) and 114 kN (M_d = 500 N m), respectively. The SDO36W and SD36W shackles utilised during the tests were produced in the reinforced versions, and they were manufactured using S480W steel. The M24 screws (regular 3-mm thread pitch) for coupling the shackle clevises were of mechanical property class 8.8, whereas the nuts were of class 8. The screws were tightened with a GEDORE torque wrench with a measuring range of up to 750 N m. Before the dynamic testing was commenced, the joints were subjected to tests under static loading to determine their static load capacity F_s following a yield z = 100 mm. An example test course of an SV32 friction prop (with two shackles, M_d = 450 N m) is presented in Fig. 3a, whereas a test of an SV32t prop (with three shackles, M_d = 500 N m) is demonstrated in Fig. 3b.

The load capacity of SV32 friction props (two shackles in the joint), with clevises tightened with a torque M_d = 450 N m, reaches a value of about 300 kN during the initial yield, and afterwards, it varies within a range of about 200-250 kN. On the other hand, the load capacity of SV32t friction props, with clevises tightened with a torque M_d = 500 N m, varies within a range of 250-300 kN during the entire yield and is characterised by greater stability compared to the SV32 props. Since the dry friction phenomenon that occurs during joint yield depends on multiple factors, that is, the shackle screw torque, the condition of the section surfaces and their state of corrosion, the smoothness of the nut and screw threads, certain variations in load capacity can often be observed even in the context of the same joint. A test result compilation for straight joints with three shackles (SV32t prop) under dynamic loading is presented in Table 1.

The SV32t sliding joint test results indicate that the increase in the ram impact velocity v_p and energy against the joint results in an increase in the surface temperature to a range of 169.6°C-234.1°C and in a greater yield z, whereas the dynamic load capacity N_d of the joints (six

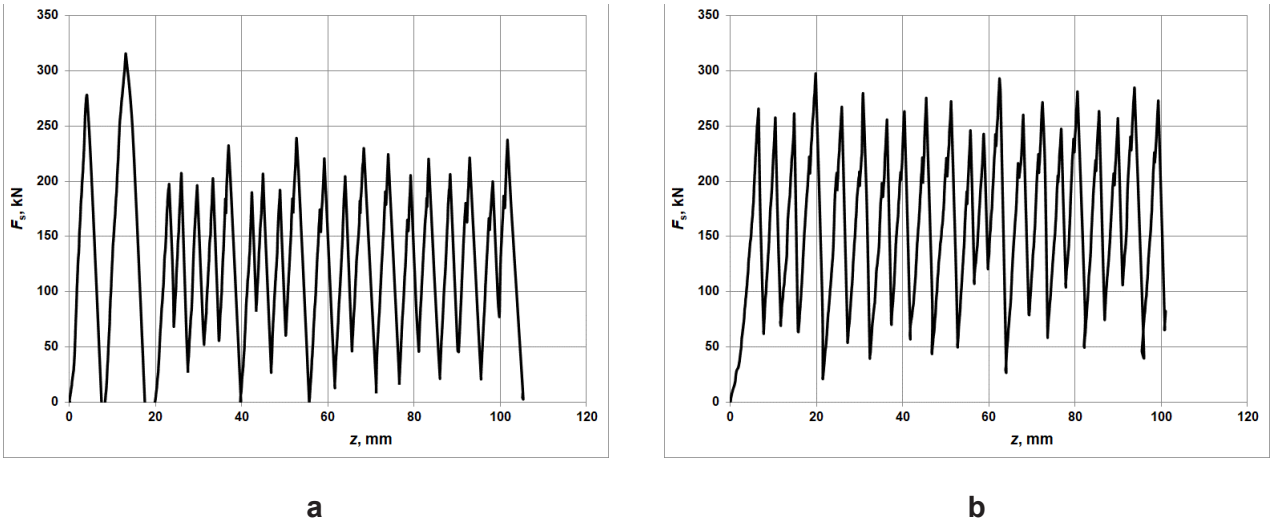

Figure 3: Courses of sliding joint static load capacity F_s: (a) SV32 – two SDO32W shackles, M_d = 450 N m; (b) SV32t – three SDO32W shackles, M_d = 500 N m.

Table 1: Result compilation of SV32t straight sliding joint tests under dynamic loading.

Test no.	v_p, m/s	z, m	E_c, J	N_d, kN	T_{max}, °C
1	2.05	140	25,556	183	169.6
2		110	23,387	213	
3		95	33,256	235	
4	2.45	155	33,256	215	175.5
5		160	33,617	210	
6		150	45,293	219	
7	2.79	230	45,293	197	234.1
8		205	43,485	212	
9		205	43,485	212	
			Average	**211**	
			Standard deviation	14	

screws – each with a tension of 114 kN) remains on a level of 211 ± 14 kN at a kinetic coefficient of friction of m_d = 0.308. The stability of the load capacity at a relatively constant and high level of the joint resisting force has a significant contribution to the increased load capacity of the support operating under the conditions of rock mass tremors and rock bursts. The surfaces marked using the dotted lines in Fig. 4b exhibit particular heating during dynamic loading, which is confirmed by the thermal images presented in Figs 5-7.

In the case of SV32t prop testing according to standard PN-G-15533:1997 at a ram height of fall of 0.7 m (v_p = 2.05 m/s), the observed joint element temperatures slightly exceed T_{max} = 150°C. On the other hand, when testing the SV32t props at impact velocities greater than what is defined for friction props in the standard in question, the observed joint element temperatures significantly exceed 200°C. Examples of such tests are presented in Figs 5-7.

Thermal traces can be observed on the section flanges in the thermal images, which are generated by the movement of the shackles along the sections. The maximum section surface temperature T = 234.1°C was recorded at an impact velocity v_p = 2.79 m/s. The moment when the joint stops sliding is marked with a dotted line in Figs 5-7. A significant decrease in the surface temperature can be observed from this point.

Tests of strongly corroded arching sliding joints obtained from ŁP10/V32/4/A frames were carried out as well, and example test results are presented in Figs 8 and 9. The strongly corroded state of the section resulted in the total yield of an arching joint with two shackles coupled with screws with a torque of 450 N m at an impact velocity v_p = 0.55 m/s, which led to a gradual increase in the surface temperature to a maximum of 207.9°C. Strong mechanical sparking can also be observed in the thermal image (Fig. 8d). The numerous corrosion products functioned as a layer facilitating the sliding of the surfaces undergoing friction, which resulted in a very low joint load capacity of 80 kN at the start of the yield that increased to about 100 kN at a later stage.

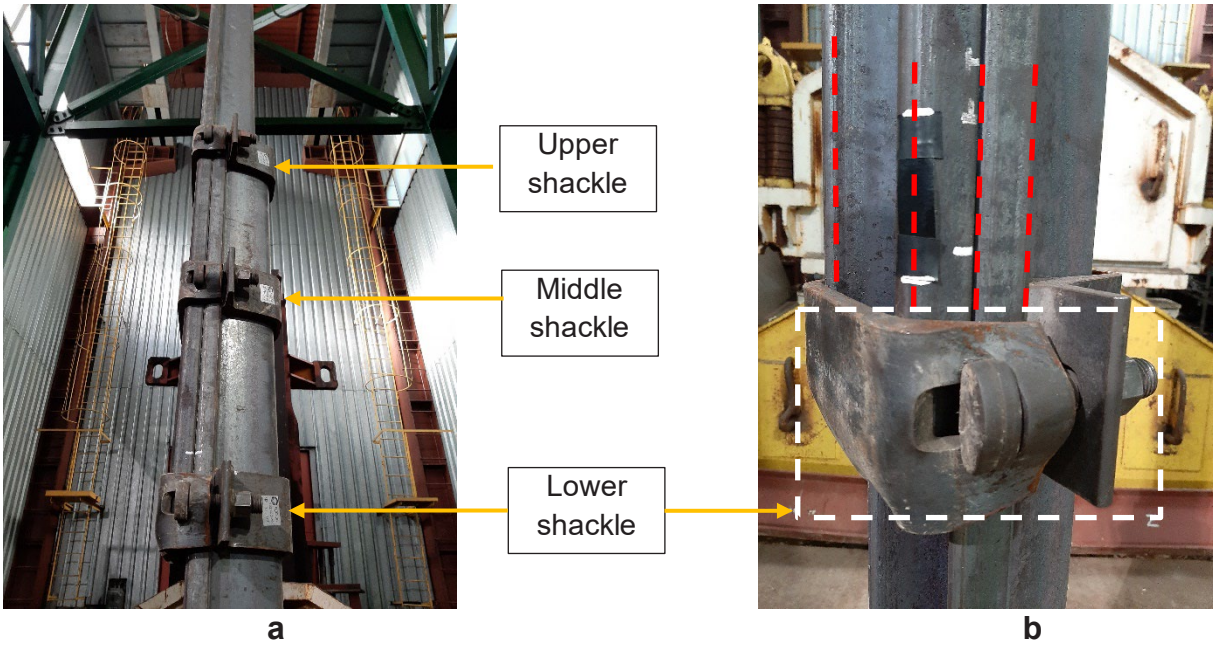

Figure 4: Pictures of sliding joints in an SV32t prop (three shackles in the joint).

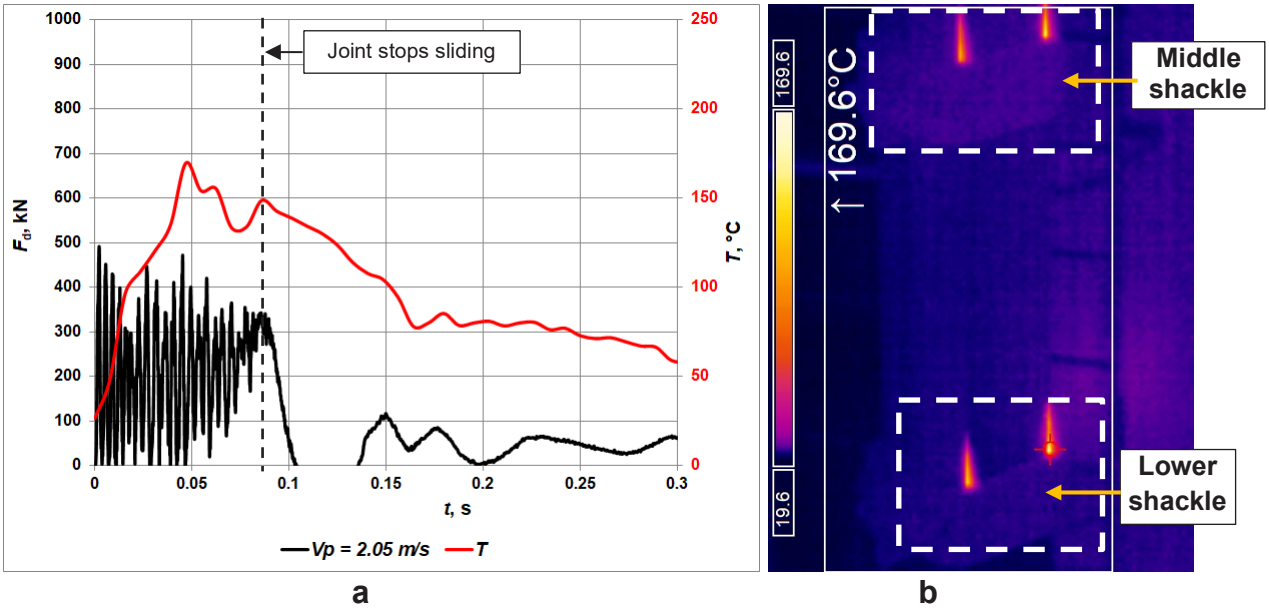

Figure 5: Course of joint force and maximum temperature at an impact velocity v_p = 2.05 m/s (a) and joint thermal image (b).

Very strong sparking accompanied by an increase in temperature to over 200°C (Fig. 9c) was also observed in the case of the same type of joint (Fig. 9) with an additional third (middle) shackle (M_d = 450 N m). The course of force as a function of time (Fig. 9a) demonstrates that despite the momentary increase in the joint resisting force to about 260 kN, there was a sudden drop in the load capacity to a level of about 70 kN, followed by a slow increase to a value of about 300 kN. This also transpired due to the influence of the corrosion products, as they happen to severely limit and hinder the correct positioning of the overlapping arching sections during the assembly of the joint. What is significant, a different character of the joint operation was observed during both the arching joint tests compared to the straight joints. The effects of this are visible in the two thermal images presented in Figs 8d and 9c.

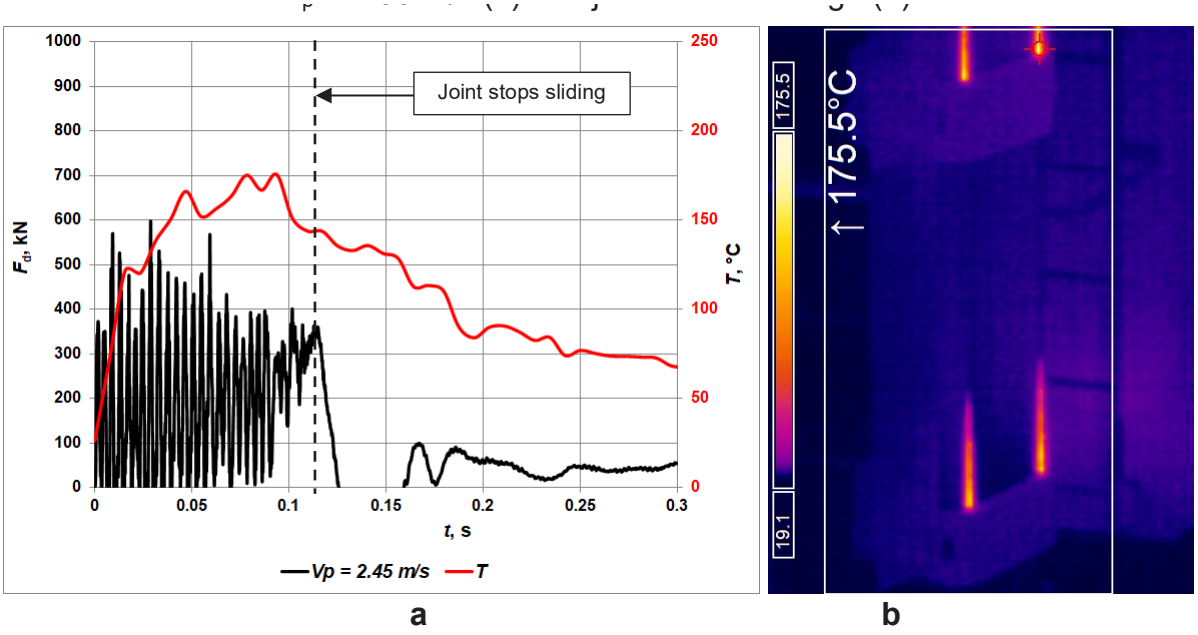

Figure 6: Course of joint force and maximum temperature at an impact velocity v_p = 2.45 m/s (a) and joint thermal image (b).

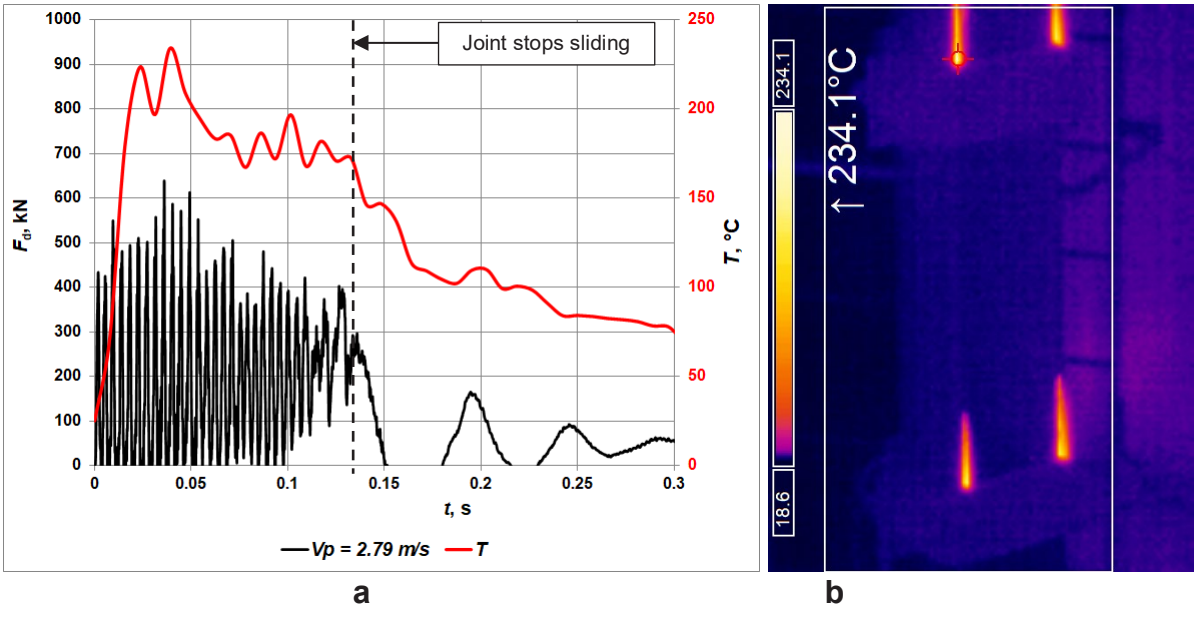

Figure 7: Course of joint force and maximum temperature at an impact velocity v_p = 2.79 m/s (a) and joint thermal image (b).

The straight and arching joints exhibit different characters of operation primarily because the tips of the arching segments 'tear' through the sections in the joint during the yield. Their key contact points are in the areas of the upper and lower shackles. Intensified sparking and increased surface temperatures are observed during a dynamic yield (Pytlik, 2020), and these result not only from the nature of the dry friction itself, but also from the tearing of the surfaces.

One solution to the problem of the excessive joint yield may be to add a fourth restraining shackle under the joint. This shackle is installed directly under the joint on a short piece of a V32 section with a length of about 150-200 mm (Fig. 10).

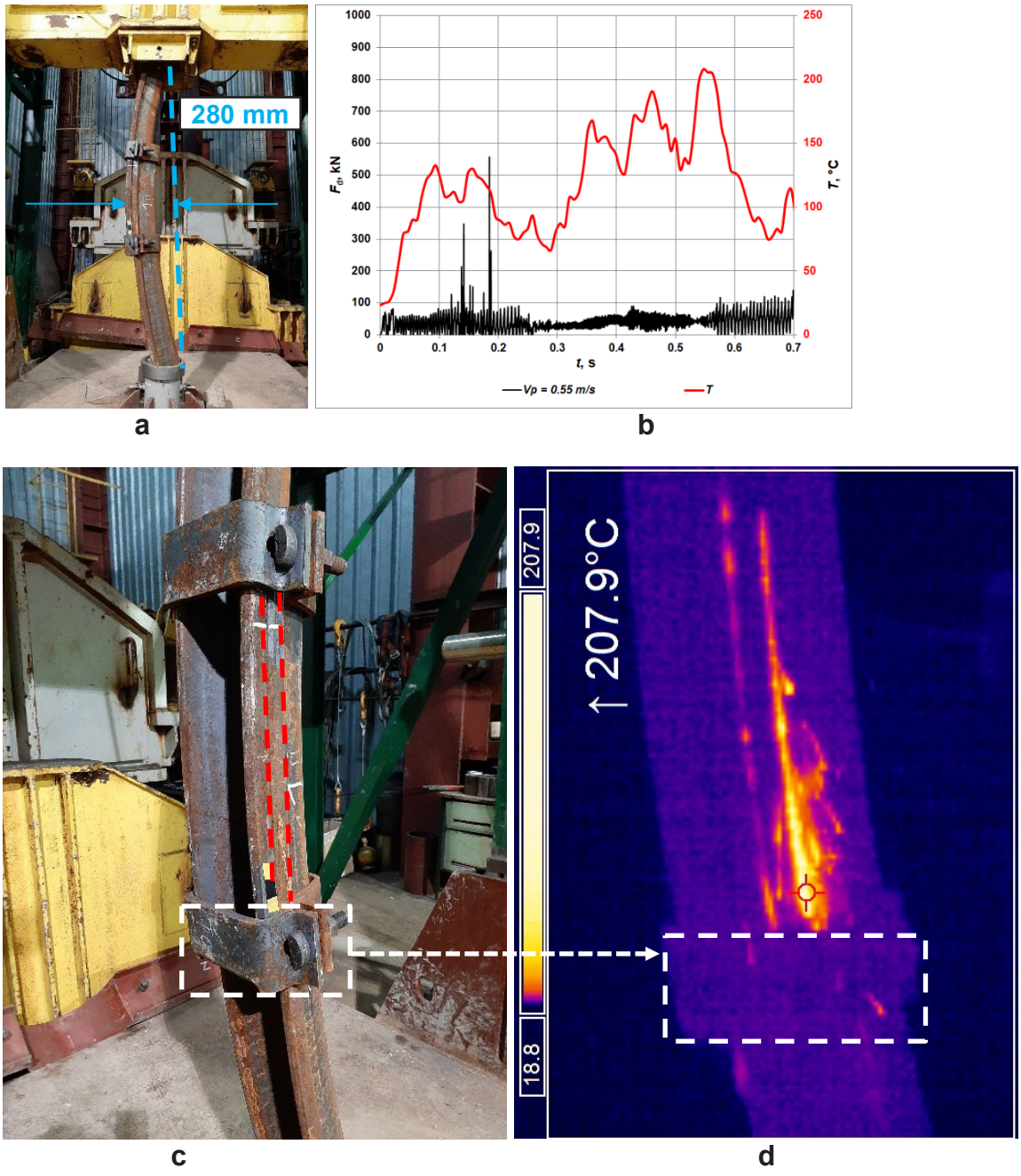

Figure 8: Arching sliding joint (a, c), course of joint force and maximum temperature at an impact velocity v_p = 0.55 m/s (b), and joint thermal image (d).

All the shackles were tightened with a lowered torque M_d = 400 N m (compared to previous testing) in order to prevent the total stiffening of the joint, which could result in its buckling. This corresponded to a single screw tension force of about 91 kN. The course of joint force and maximum temperature at an impact velocity v_p = 2.05 m/s and a thermal image of the joint with the captured maximum temperature T_{max} = 102°C are presented in Fig. 11.

It can be clearly observed that the temperature falls significantly below the standard value of T_{max} = 150°C. The four-shackle joint (eight screws – each with a tension force of 91 kN) stopped after 100 mm of yield at a dynamic load capacity N_d = 227 kN and a kinetic coefficient of friction m_d = 0.312.

The calculated values of the kinetic coefficient of friction m_d are similar to the value of the provisional

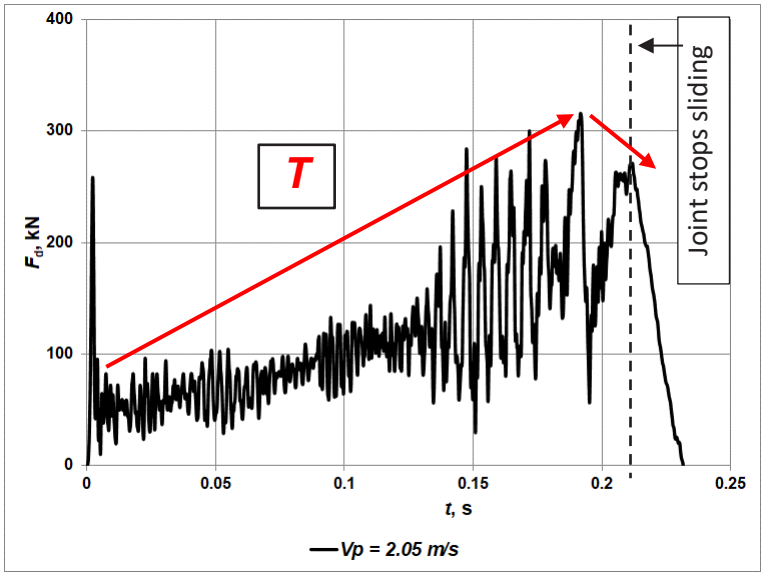

a

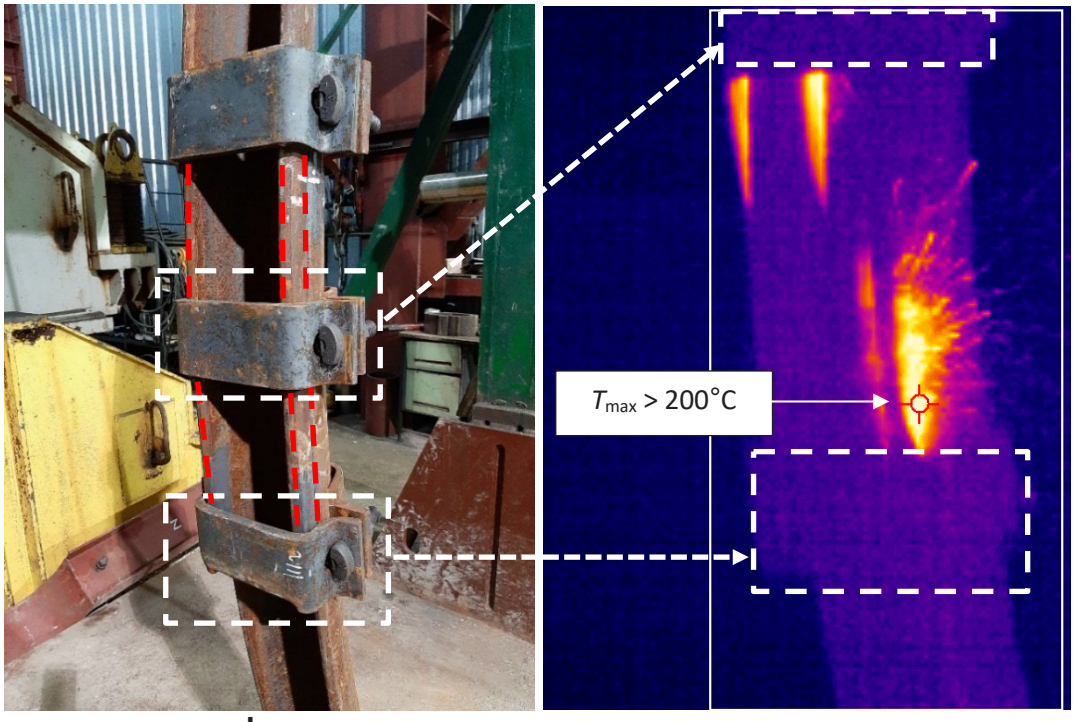

b c

Figure 9: Course of joint force and maximum temperature at an impact velocity v_p = 2.05 m/s (a), picture of an arching joint (b), and joint thermal image (c).

coefficient of friction m_z = 0.2945 formulated and calculated by Ciałkowski (1996). The publication presenting model support sliding joint tests (Horyl et al., 2019) provides a value of 0.27 for the static coefficient of friction between yielding sections. On the other hand, the model tests presented by Brodny (2012a) adopted a value of 0.3 for the kinetic coefficient of friction, whereas the tension forces in the screws calculated therein are concurrent with the screw tension forces demonstrated in this paper.

Another example of a design solution for a frictional joint, compared to a joint with a braking shackle, which significantly reduces the sliding value, is the use of a shackle with a resistance wedge (Brodny, 2012b). Such shackle causes a significant increase in the resistance force

1 – upper shackle; 2 – middle shackle; 3 – lower shackle; 4 – restraining shackle

Figure 10: SV32tw friction prop with four shackles: three shackles in the joint and one restraining shackle under the joint.

of the joint during the sliding of the sections in the friction prop. However, in the available literature, no results of surface temperature studies of the joint components have been encountered.

As the issues concerning the places of mechanical spark formation on yielding steel arch support and the formation of high-temperature places that may pose a risk of ignition of explosive gas mixtures are poorly recognised, the authors of the article had difficulty in referring to both Polish and foreign literature. The article fills a gap concerning the sparking phenomena of steel arch yielding support during dynamic loading.

4 Conclusions

Compared to the temperature T_{max} = 150°C defined in standard PN-EN ISO 80079-36:2016, the straight arching joint tests at an impact velocity v_p = 2.05 m/s revealed a slightly exceeded V32 section surface temperature, up to a maximum temperature T = 169.6°C. The impact velocity v_p = 2.05 m/s corresponds to the requirements of standard PN-G-15533:1997, which defines a requirement of 0.7 m for the ram falling height h during sliding joint tests.

Tests of straight sliding joints at impact velocities greater than what is defined in standard PN-G-15533:1997 demonstrated that the surface temperature

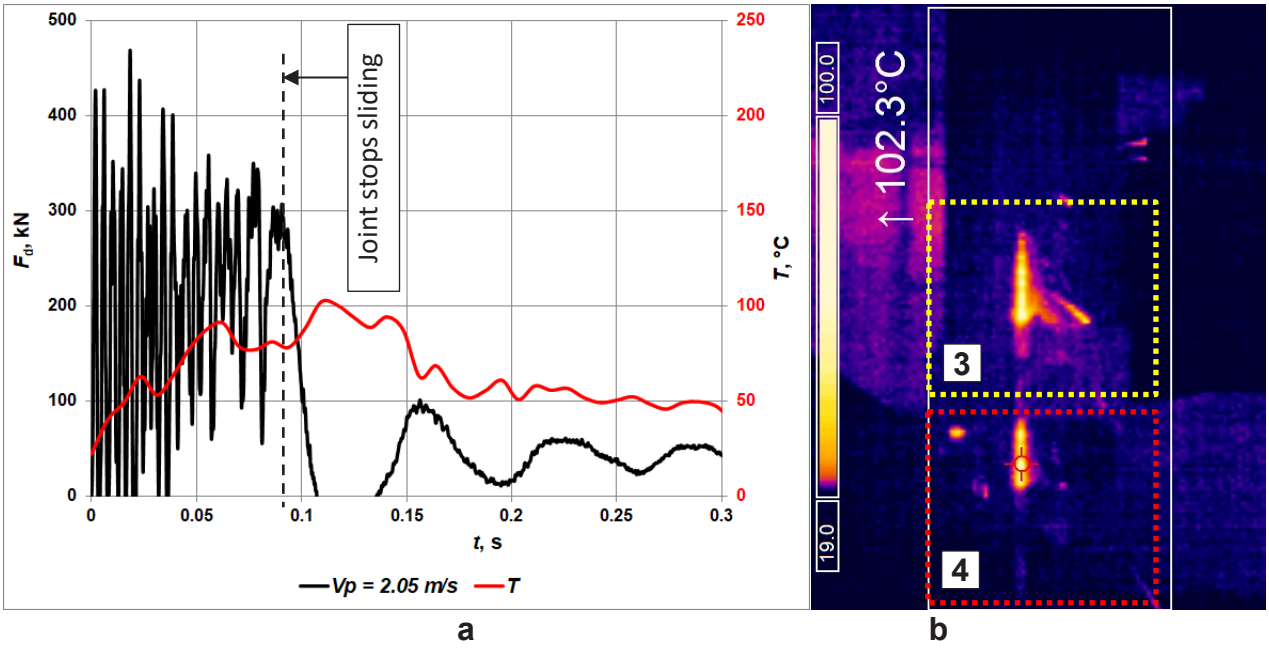

Figure 11: Course of joint force and maximum temperature at an impact velocity v_p = 2.05 m/s (a) and joint thermal image (b). 3 – lower shackle; 4 – restraining shackle.

rises significantly above the permissible temperature T_{max} = 150°C in the case of impact velocities greater than 2.45 m/s. At an impact velocity v_p = 2.79 m/s, the maximum surface temperature reached a value as high as 234.1°C. Such a situation can pose a risk of methane and coal dust ignition.

A similar situation occurred during the tests of arching sliding joints obtained from ŁP10/V32/4/A support frames. The maximum surface temperature during testing also exceeded 200°C, and strong sparking in the areas of the upper and lower shackles was observed at yield. This was primarily due to the tearing of the surfaces by the tips of the arching sections and the melting of the corrosion products as a result of the temperature increase at the contact points between the arching sections.

The temperature increase of sliding joints subjected to dynamic impact loading can be limited by preventing excessive joint yields. An additional fourth shackle restraining the movement of the joint, installed directly under the joint, is applied for this purpose in certain types of friction props (e.g. SVtw). This solution is currently not used in arching support frame joints, primarily due to economic factors. The tests demonstrated that using a fourth shackle in the joint prevents rapid joint element temperature increases as a result of excessive yielding. During the testing of straight joints with four shackles, at a torque M_d = 400 N m, dynamic load capacity N_d = 227 kN and impact velocity v_p = 2.05 m/s, the calculated kinetic coefficient of friction was m_d = 0.312. A similar kinetic coefficient of friction m_d value of 0.308 was obtained for the tests of straight joints constructed from V32 sections with three shackles, at M_d = 500 N m, N_d = 211 kN and v_p = 2.05 m/s.

In the case of steel arch support systems, the arching sections should be made with the same bend radius to limit the tearing effect of the sections in the joint, which is the primary cause of mechanical sparking. Determining such mechanical parameters of the joints that would limit yielding to a minimum and reduce sparking in the joint requires the conduction of further testing – particularly arching joint testing – involving various types of the V section and the various states of its corrosion, as well as different numbers of shackles in the joint and varied shackle screw nut torques. The aim of further research should also be to test different sliding joints: both existing on the market and new ones, with a view to minimising section slide in the joint, joint friction surface temperature and sparking. The adapted methodology is applicable to all friction straight and arch joints tested, existing on the market, under static and dynamic loading under laboratory conditions.

References

[1] Brodny J. (2012a). *Work parameter identification of sliding joints utilised in yielding steel arch support*. Wydawnictwo Politechniki Śląskiej, Gliwice (in Polish).

[2] Brodny J. (2012b). *Analysis of operation of new construction of the frictional joint with the resistance wedge*. Archives of Mining Sciences, 57(1), 209-227.

[3] Brodny J. (2013). *Analysis of operation of arch frictional joint loaded with the impact of freely falling mass*. Studia Geotechnica et Mechanica, 35(1), 59-72.

[4] Brune J. F. (2013). *The methane-air explosion hazard within coal mine gobs*. SME Transactions, 334, 376-390.

[5] Burtan Z., Stasica J., Rak Z. (2017). *The influence of natural hazards of disasters on the work safety conditions in Polish coal mining in the years 2000–2016*. Zeszyty Naukowe Instytutu Gospodarki Surowcami Mineralnymi i Energią Polskiej Akademii Nauk, 101, 7-18 (in Polish).

[6] Ciałkowski B. (1996). *Theoretical and experimental foundations of the construction of ŁP support joints for excavations at risk of rock bursts*. PhD dissertation. Główny Instytut Górnictwa, Katowice (in Polish).

[7] Cioca I. L., & Moraru R. I. (2012). *Explosion and / or fire risk assessment methodology: a common approach, structured for underground coalmine environments*. Archives of Mining Sciences, *57*(1), 53-60.

[8] Cybulski K., Dyduch Z., Hildebrandt R., Koptoń H. (2018). *Development of methane explosions in the underground experimental facilities of GIG EM Barbara*. Zeszyty Naukowe Instytutu Gospodarki Surowcami Mineralnymi i Energią PAN, 29–40 (in Polish).

[9] Dubiński J., Konopko W. (2000). *Rock bursts: evaluation, forecast, elimination*. Główny Instytut Górnictwa, Katowice (in Polish).

[10] Eckhoff R. K. (2006). *Differences and similarities of gas and dust explosions: A critical evaluation of the European 'ATEX' directives in relation to dusts*. Journal of loss prevention in the process industries, 19(6), 553-560.

[11] Gakhar S. J., Taylor S. D., Barker I., Clayton P. (2006). *Practical experience in carrying out non-electrical equipment ignition risk assessments*. In INSTITUTION OF CHEMICAL ENGINEERS SYMPOSIUM SERIES (Vol. 151, p. 422). Institution of Chemical Engineers; 1999.

[12] Ghicioi E., Paraian M., Ridzi T. I., Vatavu N., Lupu L., Jurca A. (2010a). *IMPLEMENTING NEW TOOLS FOR THE ASSESSMENT OF NON-ELECTRICAL EQUIPMENT USED IN UNDERGROUND MINES*. IN ACCORDANCE WITH THE EUROPEAN DIRECTIVE ATEX 94/9/EC, ADOPTED IN ROMANIA BY GOVERNMENT DECISION NO. 752/2004. Revista Minelor / Mining Revue, 16(1).

[13] Ghicioi E., Paraian M., Lupu L., Jurca A. M. (2010b). *NEW TOOLS FOR ASSESSMENT OF NON-ELECTRICAL EQUIPMENT INTENDED USE IN FIREDAMP UNDERGROUND MINES, RELATED TO EUROPEAN DIRECTIVE ATEX 94/9/EC, ADOPTED IN ROMANIA BY GOVERNMENT DECISION NO. 752/2004*. Annals of the University of Petrosani Mining Engineering, 11.

[14] Górny M. (2013). *History of explosion safety in Poland*. Bezpieczeństwo przeciwwybuchowe – wybrane zagadnienia. Praca zbiorowa. Główny Instytut Górnictwa, Katowice, 7-23 (in Polish).

[15] Górny M. (2017). *Ignition risk assessment of nonelectrical part of drive system*. Napędy i Sterowanie, 19, Nr 10, 82-88 (in Polish).
[16] Hao F., Liu M., Zuo W. (2014). *Coal and gas outburst prevention technology and management system for Chinese coal mines: a review*. In Mine Planning and Equipment Selection, Springer, Cham, 581-600.
[17] Horst R., Modrzik M., Ficek P., Rotkegel M., Pytlik A. (2018). *Corroded steel support friction joint load capacity studies as found in Piast-Ziemowit coal mine*. Mining–Informatics, Automation and Electrical Engineering, 56, 81-87.
[18] Horyl P, Šňupárek R., Marsalek P. (2014). *Behaviour of frictional joints in steel arch yielding supports*. Archives of Mining Sciences 59 (3), 723-734.
[19] Horyl P, Šňupárek R., Marsalek P., Pacześniowski K. (2017). *Simulation of laboratory test of steel arch support*. Archives of Mining Sciences 62 (1), 163-176.
[20] Horyl P., Šňupárek R., Maršálek P., Poruba Z., Pacześniowski K. (2019). *Parametric Studies of Total Load-Bearing Capacity of Steel Arch Supports*. Acta Montanistica Slovaca, 24(3), 213-222.
[21] Hudeček V., Zapletal P., Stoniš M., Sojka R. (2012). *New recommendations in the area of prediction and prevention of rock and gas outbursts in the Czech Republic*. Rudarsko-geološko-naftni zbornik, 25(1), 101-106.
[22] Jespen T. (2016). *ATEX—Equipment Selection. In: ATEX—Explosive Atmospheres*. Springer Series in Reliability Engineering. Springer, Cham.
[23] Jurca A. M., Vătavu N., Lupu L., Popa M. (2020). *Determining the maximum surface temperature for non-electrical equipment aiming at explosion prevention at protection*. In MATEC Web of Conferences (Vol. 305, p. 00026). EDP Sciences.
[24] Kałuża G. (2017). *Temperature measurements in the process of testing explosion-proof devices*. Maszyny Elektryczne: zeszyty problemowe Nr 1/2017 (113), 85-89 (in Polish).
[25] Krause E., Smoliński A. (2013). *Analysis and assessment of parameters shaping methane hazard in longwall areas*. Journal of Sustainable Mining, 12(1), 13-19.
[26] Krause E., Skiba J. (2014). *Formation of methane hazard in longwall coal mines with increasingly higher production capacity*. International Journal of Mining Science and Technology, *24*(3), 403-407.
[27] Lebecki K., Cybulski K., Śliz J., Dyduch Z., Wolański P. (1995). *Large scale grain dust explosions-research in Poland*. Shock Waves, 5(1-2), 109-114.
[28] Li G., Shang R. X., Yu Y. J., Wang J. Z., Yuan C. M. (2013). *Influence of coal dust on the ignition of methane/air mixtures by friction sparks from rubbing of titanium against steel*. Fuel, 113, 448-453.
[29] Petitfrere C., Proust C. (2006). *Analysis of ignition risk on mechanical equipment in ATEX*. In 2007 4th European Conference on Electrical and Instrumentation Applications in the Petroleum & Chemical Industry (pp. 1-9). IEEE.
[30] Polski Komitet Normalizacyjny (2016). *Explosive atmospheres — Part 36: Non-electrical equipment for explosive atmospheres — Basic method and requirements* PN-EN ISO 80079-36:2016-07. Warszawa (in Polish).
[31] Polski Komitet Normalizacyjny (1997). *Polish Standard: Single prop mine support. Friction props. Requirements and testing*. PN-G-15533:1997. Warszawa (in Polish).
[32] Polski Komitet Normalizacyjny (2004). *Polish Standard: Hotrolled steel sections for mining. V sections. Dimensions*. PN-H-93441-3:2004. Warszawa (in Polish).
[33] Pacześniowski K., Pytlik A. (2008). *Methodology of dynamic load capacity determination of frictional joints applied in mining support*. Prace Naukowe GIG. Górnictwo i Środowisko. Główny Instytut Górnictwa, 63-71 (in Polish).
[34] Prostański D. (2018). *Development of research work in the air-water spraying area for reduction of methane and coal dust explosion hazard as well as for dust control in the Polish mining industry*. In IOP Conference Series: Materials Science and Engineering (Vol. 427, No. 1, p. 012026). IOP Publishing.
[35] Pytlik A. (2019a). *Tests of steel arch and rock bolt support resistance to static and dynamic loading induced by suspended monorail transportation*. Studia Geotechnica et Mechanica 41 (2), 81-92.
[36] Pytlik A. (2019b). *Comparative bench testing of steel arch support systems with and without rock bolt reinforcements*. Archives of Mining Sciences, 64.
[37] Pytlik A. (2020). *Experimental Studies of Static and Dynamic Steel Arch Support Load Capacity and Sliding Joint Temperature Parameters During Yielding*. Archives of Mining Sciences, 469-491.
[38] Pytlik A., Tokarczyk J., Frąc W., Michalak D. (2021). *Explosive atmosphere ignition source identification during mining plant suspended monorail braking unit operation*. ACTA MONTANISTICA SLOVACA, 26(2), 338-351.
[39] Rogers, R. L. (2003). *Development of European standards: non-electrical equipment for use in explosive atmospheres*. In INSTITUTION OF CHEMICAL ENGINEERS SYMPOSIUM SERIES (Vol. 149, pp. 461-476). Institution of Chemical Engineers; 1999.
[40] Shao X. Q., Ma X. M. (2012). *The design of Coal mine construction safety monitoring system*. In Applied Mechanics and Materials (Vol. 174, pp. 3459-3462). Trans Tech Publications Ltd.
[41] Shepherd J., Rixon L. K., Griffiths L. (1981). *Outbursts and geological structures in coal mines: a review*. In International Journal of Rock Mechanics and Mining Sciences & Geomechanics Abstracts, Vol. 18, No. 4, Pergamon, 267-283.
[42] Song W., Cheng J., Wang W., Qin Y., Wang Z., Borowski M., Wang Y., Tukkaraja, P. (2021). *Underground mine gas explosion accidents and prevention techniques–an overview*. Archives of Mining Sciences, 66(2), 297-312.
[43] Takla G., Vavrusak Z. (1999). *Coal Seam Gas Emissions from Ostrava—Karvina Collieries in the Czech Republic during Mining and after Mines Closure*. In Coalbed Methane: Scientific, Environmental and Economic Evaluation, Springer Dordrecht, 395-409.
[44] Thurnherr P., Schwarz G., Oberhem H. (2007). *Non-Electrical Equipment for Potentially Explosive Atmospheres*. In 2007 IEEE Petroleum and Chemical Industry Technical Conference (pp. 1-9). IEEE.
[45] Trenczek S. (2015). *Methane ignitions and explosions in the context of the initials related to technical and natural hazards*. Przegląd Górniczy, 71(2), 87-92 (in Polish).
[46] Yuan L. (2016). *Control of coal and gas outbursts in Huainan mines in China: A review*. Journal of Rock Mechanics and Geotechnical Engineering, 8(4), 559-567.

[47] Zhang L., Wang H., Chen C., Wang P., Xu L. (2021). *Experimental study to assess the explosion hazard of CH4 / coal dust mixtures induced by high-temperature source surface*. Process Safety and Environmental Protection, 154, 60-71.